Check for updates

Angewandte Chemie Novit

Angewandte Novit Chemie

GDCh German Chemical Society

RESEARCH ARTICLE OPEN ACCESS

Unexpected {Pu_{60}} Cage Cluster Units in New Plutonium(VI) Oxido-Hydroxides

David Fellhauer[1] | Olaf Walter[2] | Jörg Rothe[1] | Kathy Dardenne[1] | Dieter Schild[1] | Roland Meier[1] | Philipp Müller[1] | Yongheum Jo[1,3] | Xavier Gaona[1] | Marcus Altmaier[1] | Horst Geckeis[1]

[1]Institute for Nuclear Waste Disposal, Karlsruhe Institute of Technology, Karlsruhe, Germany | [2]Joint Research Centre Karlsruhe, European Commission, Karlsruhe, Germany | [3]Department of Nuclear Engineering, Hanyang University, Seoul, Republic of Korea

Correspondence: David Fellhauer (david.fellhauer@kit.edu)

Received: 26 November 2025 | **Revised:** 24 January 2026 | **Accepted:** 3 March 2026

Keywords: cage clusters | hydrolysis | plutonium(VI) | polyoxometalates | truncated dodecahedron

EDITORIAL SUMMARY

Inorganic metal-oxygen clusters are structures where metal cations are coordinated by oxide, hydroxide, or peroxide anions. These assemblies bridge the gap between molecular complexes and extended solid-state structures, with the largest examples containing up to 500 metal atoms. Fellhauer and colleagues have identified two unique spherical plutonium(VI) cage structures, each containing 60 plutonium polyhedra. This discovery is unexpected, as there are no comparable analogs for uranium(VI) or neptunium(VI), despite much more extensive research. Although many inorganic clusters have a topology based on Archimedean solids, the Pu_{60} clusters appear to be the first based on the truncated dodecahedron. The Scientific Advisory Committee of Angewandte Chemie Novit recognizes this study as a major advancement in the study of actinide clusters, with wide-reaching effects on actinide speciation, self-assembly processes, and inorganic cage chemistry.

ABSTRACT

Plutonium (Pu), a prominent representative of the 5f-block actinides, is a redox active element. Pu(III)-Pu(VI) are the four thermodynamically stable redox states in aqueous solution. For Pu(VI), hydrolysis reactions in NaCl solutions start in weakly acidic conditions ($pH_c \approx 5$); increasing the alkalinity typically yields supersaturated solutions that are metastable with respect to the formation of Pu(VI)-oxido-hydroxide solid-phases. We show that needle- and platelet-like crystals of Pu(VI) form in strongly alkaline NaCl-NaOH solutions. Detailed characterization reveals that both are built from surprisingly novel, spherical $[(PuO_2)_{60}O_{20}(OH)_{120}]^{40-}$ cage clusters that are interlinked by sodium ions. The topology of the {Pu_{60}} units resembles a truncated dodecahedron (*Archimedean* solid), representing a rather uncommon case in structural chemistry. Each cage contains 20 identical trimeric subunits that correspond closely to the trimeric Pu(VI) solution complex predominant under the crystallization conditions. This indicates that both solids form by a self-assembly from the precursor solution species, highlighting the trimer as a hitherto not considered principal building block in actinide cage cluster chemistry. The present study also addresses an open issue dating back to one of the earliest studies on Pu(VI) hydrolysis from 1949, which first described the two crystal types without a clear structural interpretation.

This is an open access article under the terms of the Creative Commons Attribution License, which permits use, distribution and reproduction in any medium, provided the original work is properly cited.

© 2026 The Author(s). *Angewandte Chemie Novit* published by Wiley-VCH GmbH on behalf of Gesellschaft Deutscher Chemiker (GDCh; the German Chemical Society).

1 | Introduction

Inorganic metal-oxygen clusters are assemblies of heteroatomic $\{MO_x\}$ units, where the metal cation M is coordinated by oxo/oxido (O^{2-}), hydroxo (OH^-) or peroxido (O_2^{2-}) anions. While the minimum number of metal ions in a discrete cluster is three, giant representatives contain several hundred atoms (current maximum ≈ 500) [1, 2]. Standing between molecular complexes and extended solid-state structures, they exhibit fascinating physical-chemical properties [3, 4]. Many inorganic metal-oxygen clusters form in aqueous solutions by self-assembly of the predominant metal solution complexes. Detailed knowledge of the solution speciation of the precursors is therefore crucial for a comprehensive understanding of cluster formation [5]. Large clusters are of particular interest because they often mimic the highly symmetric, spherical polyhedra derived from Platonic and Archimedean solids [6]. Classical representatives are polyoxometalates (POMs) of d-block elements (V, Nb, Mo, W, etc.). In the last two decades, research has extended to oxygen clusters and POMs of 5f-block actinides (An), which can be roughly divided into An-containing clusters (built from non-actinide metals, with the An as a minor component) and An-oxo-clusters (in which the actinide is the main building block) [7]. The most extensive group of large clusters in the latter subset consists of uranium(VI) (U(VI)) peroxide cage structures, largely discovered by the group of P. C. Burns and now numbering about 60 compounds [7–11]. Most are built from uranyl penta- and hexagonal bipyramidal polyhedra that contain two peroxido and one to two additional ligands (hydroxide, oxalic acid, (pyro)phosphate, organic phosphonates). Peroxide is considered essential because the U-O_2-U bridges linking the uranyl units are highly pliable, enabling the curvature required for spherical cages [11]. Given the large number of reported U(VI) peroxide clusters and the analogous chemistry of actinides in the same oxidation state, it is surprising that Pu(VI) peroxide clusters have not been identified [12, 13]. However, their formation is highly challenging because aqueous Pu(VI) is rapidly reduced to lower oxidation states by peroxide, highlighting the strong redox sensitivity of Pu species in water.

In contrast to peroxo systems, U(VI) oxide clusters that contain more than 16 U(VI) cations (i.e., more than the number of U(VI) ions in the smallest known U(VI)-O_2 cage) and where the U(VI) polyhedral building blocks contain only the intrinsic building blocks of water, $H_2O/OH^-/O^{2-}$, are practically unknown [9, 11]. Instead, most reported U(VI) solids with $H_2O/OH^-/O^{2-}$ ligands adopt one- and 2D structures (infinite chains or sheets) [14]. This suggests that uranyl polyhedra coordinated solely by these ligands favor extended "linear" structures rather than discrete spherical cages, lacking the pliability conferred by peroxide. For plutonium (Pu), a prominent representative of the transuranium elements and notorious for its unique physicochemical properties, only a few structures containing Pu-oxygen clusters with ≥ 16 Pu ions have been documented [9, 15, 16]. While such clusters are absent for Pu(III), Pu(V) and Pu(VI), a notable Pu(IV) example is the $[Pu_{38}O_{56}]^{40+}$ central core unit found in $Li_{14}(H_2O)_n[Pu_{38}O_{56}Cl_{54}(H_2O)_8]$ and $Li_2[Pu_{38}O_{56}Cl_{42}(H_2O)_{20}]\cdot 15H_2O$ [17, 18]. Analogous $\{An_{38}O_{56}\}$ core units have later been reported for U(IV) and Np(IV) species [19, 20].

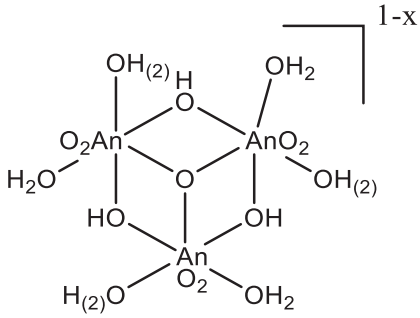

FIGURE 1 | Structural formula of trimeric An(VI) hydrolysis species $(AnO_2)_3(\mu_3\text{-}O)(\mu_2\text{-}OH)_3(t\text{-}OH)_x(t\text{-}H_2O)_{6-x}^{1-x}$ (x = 0-3), briefly assigned as $(AnO_2)_3(OH)_{5+x}^{1-x}$ or "(3,5+x)" [27].

A relevant difference between aqueous systems of U(VI) and Np(VI) versus Pu(VI) is the metastability of Pu(VI) at T = 25°C toward the formation of solid (hydr)oxide compounds from oversaturation conditions. While U(VI)/Np(VI) precipitate readily upon addition of alkali hydroxides around near-neutral pH, Pu(VI) remains predominantly as dissolved polyatomic $(PuO_2)_x(OH)_y^{2x-y}$ species over the pH range 5-14, even at millimolar Pu(VI) concentrations and over extended periods [21–23]. The results of several studies confirm that dimeric $(PuO_2)_2(OH)_2^{2+}$ and trimeric $(PuO_2)_3(OH)_5^+$ are important species at pH ≈ 5-7 [22, 24, 25]. However, a clear picture of the polynuclear Pu(VI)-OH species dominating at pH > 7 was lacking for a long time. To fill this gap we recently analyzed the speciation of metastable Pu(VI)-OH complexes in 1.0 mol·L^{-1} NaCl-NaOH solutions as a function of pH_c (pH_c = 2-14) and [Pu(VI)] concentration ([Pu(VI)] ≈ 10^{-5} to 10^{-2} M) by Vis/NIR and XAFS spectroscopy [26]. By systematic analysis of the dependencies on pH_c and [Pu(VI)] (slope analysis) in ≈ 200 sample spectra, we demonstrated that a class of trimeric polyoxometalates $(PuO_2)_3(\mu_3\text{-}O)(\mu_2\text{-}OH)_3(t\text{-}OH)_x(t\text{-}H_2O)_{6-x}^{1-x}$ (x = 0-3) are the predominant Pu(VI) species over wide pH_c and [Pu(VI)] ranges (Figure 1) and derived the corresponding thermodynamic hydrolysis constants (the Pourbaix diagram in Figure 2 summarizes important results from that work, that is, the predominance fields of relevant species) [27]. Under certain conditions the formation of brownish needle-like **(I)** and smaller blackish platelet-like **(II)** crystalline Pu(VI)-OH solids was observed.

In the present work we elucidate the nature of these two solid compounds and their relation to the predominant Pu(VI) solution species.

2 | Results and Discussion

Figure 2 summarizes the formation conditions of the crystalline Pu(VI)-OH precipitates observed in selected Vis/NIR samples from our related study. The experiments used 0.4-2.0 mL of 1.0 mol·L^{-1} NaCl(ClO_4)-NaOH with pH_c = 13-14 and [Pu(VI)] ≈10^{-3} to 10^{-2} M, corresponding to Pu inventories of 0.2 to 1.5 mg (sections 2.1-2.2 of the Supplementary Information). Compounds **(I)** and **(II)** crystallize within a few days at high [Pu(VI)] ≈ ≥ 1·10^{-3} mol·L^{-1} and pH_c > 12.8 [26]. No systematic dependence between the solution conditions and the initial prevalence of a crystal type was observed; however, in several samples a

25109537, 2026, 1, Downloaded from https://onlinelibrary.wiley.com/doi/10.1002/anov.70018, Wiley Online Library on [09/04/2026]. See the Terms and Conditions (https://onlinelibrary.wiley.com/terms-and-conditions) on Wiley Online Library for rules of use; OA articles are governed by the applicable Creative Commons License

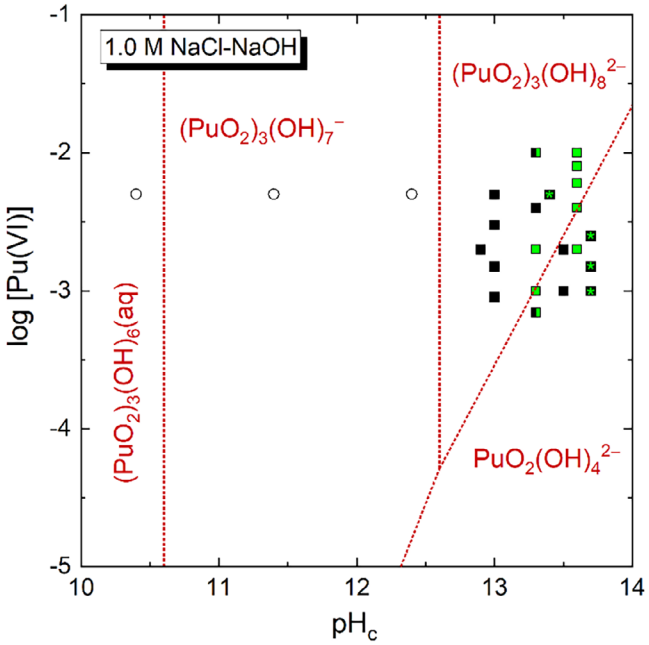

FIGURE 2 | Formation conditions of needle-like (I) (solid black squares) and platelet-like (II) (solid green squares) Na-Pu(VI)-O(H) crystals with respect to the predominance fields of the metastable Pu(VI)-OH solution species [26]. Green asterisks indicate that the initially formed (I) transformed into (II) within about 1 year. No significant solid-phase formation was observed in the three samples indicated by open circles.

transformation of initially formed needles **(I)** into platelets **(II)** occurred after ≈1 a, indicating that **(II)** is thermodynamically more stable. In samples with $10 \leq pH_c \leq 12.4$ and high [Pu(VI)] = $5{\cdot}10^{-3}$ mol·L^{-1}, no significant solid-phase formation was detected even after ≈ ½ year of equilibration. Correlating the synthesis conditions with the predominance fields of the different Pu(VI)-OH aqueous species reveals that **(I)** and **(II)** form preferentially when the complex $(PuO_2)_3(OH)_8^{2-}$ is predominant or present at high concentration (Figure 2). Representative photographs, optical microscope images, results from scanning electron microscopy with energy dispersive x-ray analysis (SEM-EDX), visible-near-infrared (Vis/NIR) and x-ray absorption fine structure (XAFS) spectroscopy, and single-crystal x-ray diffraction (SC-XRD) are summarized in sections 2.3–2.9 (Supplementary Information).

Compound **(I)** crystallizes in the monoclinic space group C2/c (no. 15), whereas the platelets **(II)** are cubic Pa−3 (no. 205) [28]. Both are built from spherical cluster units $[(PuO_2)_{60}(O)_{20}(OH)_{120}]^{40-}$, which are charge-balanced and interconnected by sodium ions. The overall topology of the $\{Pu_{60}\}$ cage clusters is identical in **(I)** and **(II)** and is shown in Figure 3. Details of the SC-XRD evaluation (including the assignment of oxygen atoms as oxo, hydroxo, and oxido ligands), the total stoichiometries of **(I)** and **(II)**, and the structural properties of the sodium ions are discussed in section 2.8 (Supplementary Information).

A single cluster unit in **(I)** and **(II)** contains 12 [10]-membered and 20 [3]-membered rings of plutonyl pentagonal bipyramids, giving 12 decagonal (non-occupied) and 20 triangular (occupied) topological faces. The clusters comprise 60 vertices defined by the Pu ions and 90 edges (3/2 per Pu unit) defined by the axes that connect neighboring Pu ions. These topological axes simplify the real connections between two Pu ions, which occur by sharing two equatorial μ_2-OH ligands and therefore do not represent direct bonds. Based on these properties, the topology of the cluster units resembles a truncated dodecahedron. The overall symmetry of the $\{Pu_{60}\}$ units, however, is lower than that of the corresponding ideal *Archimedean* solid (I_h), a fact that can be illustrated by comparing the dimensions of the large decagonal faces. In the ideal *Archimedean* solid, all decagonal faces are identical, whereas **(II)** contains two structurally different faces. Their dimensions are quite regular: Pu-Pu distances between opposite Pu atoms in a face range from 12.19–12.45 Å (average 12.31 ± 0.08 Å), so opposite edges run almost parallel. In **(I)** the six structurally unique faces show a larger variety (Pu-Pu = 11.28–13.02 Å, average 12.21 ± 0.34 Å); some faces appear more roundish, others already oval (see section 2.10, Supplementary Information). The outer diameters of a cluster unit are ≈ 25 Å for **(I)** and 26 Å for **(II)**, comparable to the $\{U_{60}\}$ peroxide cage clusters $[(UO_2)_{60}(O_2)_{60}(OH)_{60}]^{60-}$ (d ≈ 24 Å) and $[(UO_2)_{60}(O_2)_{60}(C_2O_4)_{30}]^{60-}$ (d ≈ 27 Å), both of which exhibit truncated icosahedral topologies [30, 31]. Dodecahedral ligand coordination is not uncommon in mononuclear complexes of heavier elements, and truncated dodecahedral crystal morphologies can be obtained by shape-selective growth of nanoparticles ("tailoring") [32]. Nevertheless, inorganic cage structures with a truncated dodecahedral topology appear to be unique; apart from the present **(I)** and **(II)**, we found no further examples [6, 33].

In addition to the cage composition $[(PuO_2)_{60}(O)_{20}(OH)_{120}]^{40-}$, the SC-XRD analysis identified several lighter elements (Na^+, H_2O/OH^-) directly bonded to the $\{Pu_{60}\}$ units. A complete description of the cage's internal chemistry (including the center region) could not be deduced because the potentially present elements were not defined crystallographically. Owing to the high anionic charge and large open faces, we expect the cage to be filled with matrix components (H_2O, Na^+, Cl^-, OH^-, or even Pu(VI) species). Dedicated studies on the U(VI)-peroxide system have shown that these internal species elements stabilize the cages, can exchange with the surrounding medium, and may initially even template the cluster assembly—particularly counter alkali cations [34]. Future work should provide concrete insights into the internal composition of the present Pu(VI) system.

Out of the 60 Pu polyhedra of a $\{Pu_{60}\}$ cluster unit, 30 in **(I)** and 10 in **(II)** are crystallographically asymmetric. All have the same formal coordination environment, being *di*-oxo-plutonyl(VI) pentagonal bipyramids $(PuO_2)O(OH)_4$. Two Pu = O bonds form the almost linear plutonyl center unit. The latter is coordinated in the equatorial plane by one μ_3-oxido (O^{2-}) and four μ_2-hydroxo (OH^-) ligands, which bridge neighboring plutonyl sites. The mononuclear Pu polyhedra may be formally regarded as the principle building blocks of the $\{Pu_{60}\}$ clusters, but a more comprehensive picture emerges from the twenty trimeric Pu subunits present in the cages. Two of the μ_2-OH and the μ_3-O of a $(PuO_2)O(OH)_4$ polyhedron are shared with two neighboring Pu sites to build a trimer, whereas the remaining two μ_2-OH ligands connect to a Pu polyhedron in a neighboring trimer, thereby interlinking the trimeric units (Figure 3 and Figure 4). The twenty trimers are all identical, described as

25109537, 2026, 1, Downloaded from https://onlinelibrary.wiley.com/doi/10.1002/anov.70018, Wiley Online Library on [09/04/2026]. See the Terms and Conditions (https://onlinelibrary.wiley.com/terms-and-conditions) on Wiley Online Library for rules of use; OA articles are governed by the applicable Creative Commons License

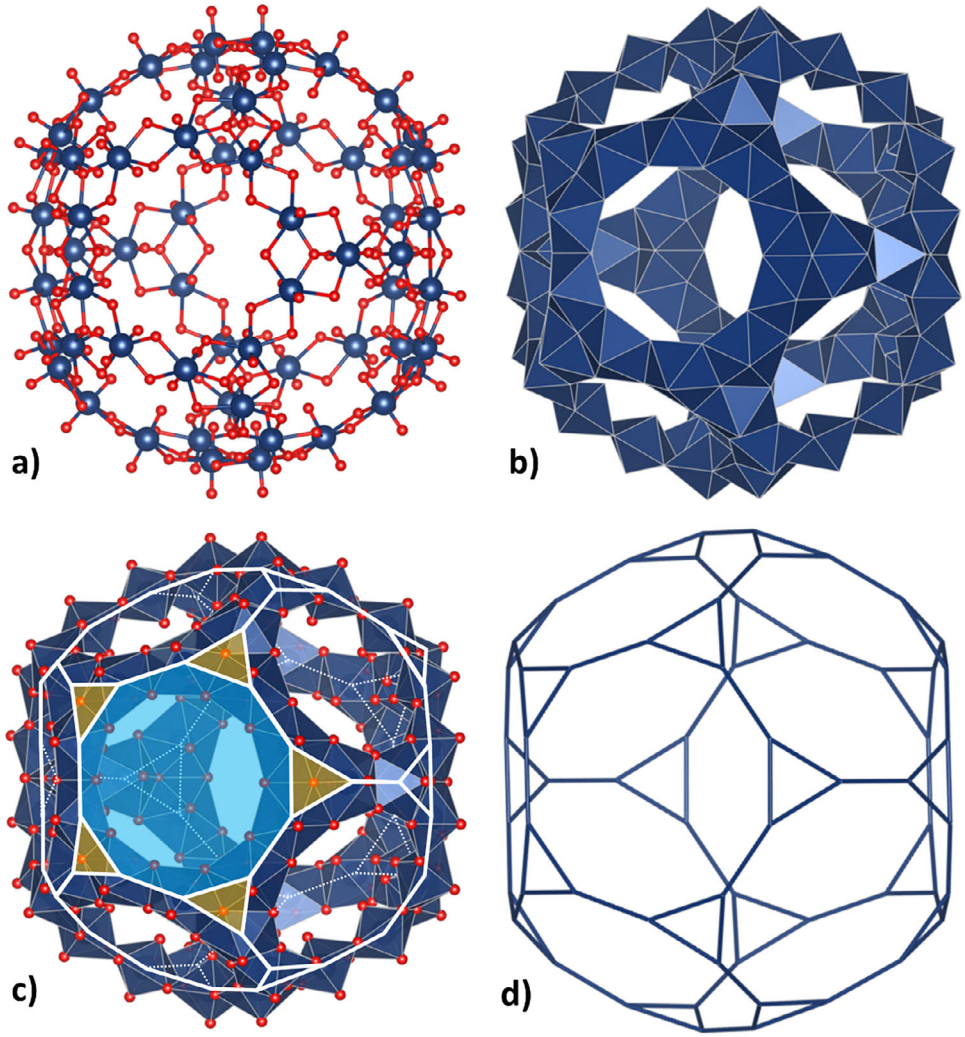

FIGURE 3 | Structure of the $\{Pu_{60}\}$ cluster units in (I) and (II) in ball-and-stick (a) and polyhedral (b) presentations with Pu in blue and O in red [29]. The overall diameters are approx. 25 and 26 Å, respectively. Graph (c) highlights the positions of selected [10]-membered and [3]-membered rings and the corresponding decagonal and trigonal faces of the truncated dodecahedral topology. In the plutonium skeleton presentation (d), topological vertices and edges represent Pu ions and axes connecting them, respectively. Graphs (a) to (d) are based on the crystal structure of compound (II). The $\{Pu_{60}\}$ units in (I) are topologically analog but show a greater degree of structural distortion.

$(PuO_2)_3(\mu_3\text{-}O)(\mu_2\text{-}OH_{(in)})_3(\mu_2\text{-}OH_{(out)})_{6/2}{}^{2-}$, where the indices *in* and *out* assign OH groups inside and outside a trimeric subunit.

Table 1 summarizes the interatomic distances and angles of **(I)** and **(II)** based on SC-XRD results. Average distances d(Pu-μ_2-OH) differ slightly for μ_2-OH ligands located inside versus outside a trimeric subunit, while deviations are even more pronounced for the d(Pu-Pu) distances between two neighboring Pu ions that belong either to the same trimer or to different trimers. Structural parameters derived from room temperature Pu L_3-edge XAFS measurements for **(I)** and **(II)** are in good qualitative agreement with the SC-XRD results and are shown for comparison in Table 2. Compared to the unhydrolyzed, mononuclear Pu(VI) aquo ion, $PuO_2(H_2O)_5{}^{2+}$ (measured as a reference during the same EXAFS beamtime), the plutonyl units in **(I)** and **(II)** exhibit significantly shorter distances $d_{Pu\text{-}Oeq}$ to the equatorial oxygen, and clearly show Pu-Pu backscattering. While the plutonyl units of **(I)** and **(II)** display two well-separated shells for the equatorial oxygen (the short-distance contribution from the μ_3-oxido ligands and the long-distance contribution from the μ_2-OH ligands), the Pu(VI) aquo ion shows only a single O_{eq} shell corresponding to the five coordinated H_2O ligands and lacks any Pu-Pu backscattering signal. Details of the XAFS are provided in section 2.7 (Supplementary Information). The average $d_{Pu\text{-}O}$ and $d_{Pu\text{-}Pu}$ distances and O = Pu = O angels are almost identical in the $\{Pu_{60}\}$ clusters of **(I)** and **(II)**, with the former displaying a distinctly larger range owing to its lower symmetry.

The average distances d(Pu-O_{ax}), d(Pu-μ_3-O), d(Pu-μ_2-$OH_{(in)}$), d(Pu-μ_2-$OH_{(out)}$), d($Pu_{(in)}$-$Pu_{(in)}$) in a trimeric unit are identical to the total mean values in the respective $\{Pu_{60}\}$ clusters of **(I)** and **(II)** within Δ = 0.03 Å, despite the larger number of crystallographically distinct Pu atoms (30 in **(I)** and 10 in **(II)**). The high crystallographic homogeneity embodied in the trimers underpins their relevance as structural building blocks rather than the mononuclear Pu polyhedra.

25109537, 2026, 1, Downloaded from https://onlinelibrary.wiley.com/doi/10.1002/anov.70018, Wiley Online Library on [09/04/2026]. See the Terms and Conditions (https://onlinelibrary.wiley.com/terms-and-conditions) on Wiley Online Library for rules of use; OA articles are governed by the applicable Creative Commons License

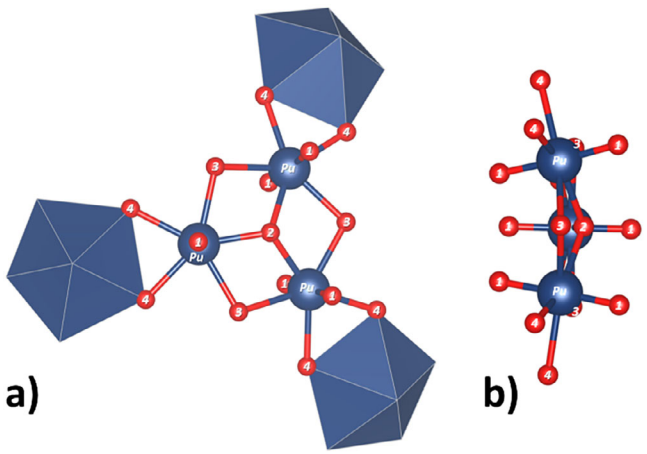

FIGURE 4 | Excerpt of the structure of the {Pu_{60}} cluster units in (I) and (II), highlighting the trimeric building blocks [29]. Top view on the convex side (a) and side view (b) revealing the curvature of the trimer. Assignment of the O atoms: 1 = O_{ax}, 2 = μ_3-O, 3 = μ_2-$OH_{(in)}$ (inside the trimer), 4 = μ_2-$OH_{(out)}$ (outside the trimer). Sodium atoms are not displayed.

TABLE 1 | Average interatomic distances and angles in the {Pu_{60}} cluster units of (I) and (II), including the 1σ standard deviation and the range (absolute min/max values) in brackets, obtained from SC-XRD results. Indices (in) and (out) are discussed in the text.

	(I)	(II)
d(Pu-O_{ax}) (Å)	1.75 ± 0.05 (1.65–1.89)	1.77 ± 0.02 (1.75–1.81)
d(Pu-μ_3-O) (Å)	2.23 ± 0.05 (2.10–2.33)	2.25 ± 0.02 (2.23–2.30)
d(Pu-μ_2-$OH_{(in)}$) (Å)	2.41 ± 0.04 (2.30–2.51)	2.42 ± 0.01 (2.40–2.45)
d(Pu-μ_2-$OH_{(out)}$) (Å)	2.38 ± 0.04 (2.26–2.47)	2.38 ± 0.02 (2.35–2.41)
d($Pu_{(in)}$-$Pu_{(in)}$) (Å)	3.74 ± 0.02 (3.70–3.78)	3.77 ± 0.02 (3.74–3.80)
d($Pu_{(in)}$-$Pu_{(out)}$) (Å)	3.82 ± 0.03 (3.76–3.87)	3.84 ± 0.03 (3.82–3.89)
< O=Pu=O (°)	177.4 ± 1.7 (170.8–179.7)	177.4 ± 0.6 (176.5–178.5)

TABLE 2 | Structural parameters for the solid compounds (I) and (II), and for 3.2·10^{-3} mol·L^{-1} Pu(VI)O_2^{2+} in aqueous 0.016 M $HClO_4$, obtained from Pu L_3-edge EXAFS.

	(I)	(II)	Pu(VI)O_2^{2+}
d(Pu-O_{ax}) (Å)	1.81 (N = 2)	1.82 (N = 2)	1.75 (N = 2)
d(Pu-O_{eq_1}) (Å)	2.12 (N = 0.5)	2.18 (N = 1.5)	2.46 (N = 3.6)
d(Pu-O_{eq_2}) (Å)	2.32 (N = 4.3)	2.38 (N = 3.9)	
d(Pu-Pu)$_{av}$ (Å)	3.78 (N = 1.5)	3.78 (N = 1.5)	n/a

The trimeric subunits in **(I)** and **(II)** closely resemble the structures of the aqueous An(VI) hydrolysis species, "$(AnO_2)_3(OH)_{5+x}^{1-x}$" = $(AnO_2)_3(\mu_3\text{-O})(\mu_2\text{-OH})_3(t\text{-OH})_x(t\text{-}H_2O)_{6-x}^{1-x}$ (x = 0-3), which are known to dominate in solutions at moderate to high An(VI) concentrations, including the recently investigated Pu(VI) species [25, 26, 35]. Consequently, the formation of **(I)** and **(II)** can be rationalized as the self-assembly of twenty aqueous Pu(VI) trimeric precursor ions, specifically the divalent (3,8) complex $(PuO_2)_3(\mu_3\text{-O})(\mu_2\text{-OH})_3(t\text{-OH})_3(t\text{-}H_2O)_3^{2-}$. Condensation of the terminal OH/H_2O ligands links the polynuclear units, in line with observations from other polyoxometalate systems [3, 4]. Condensation of hydrolyzed actinide species to form larger oligomers and assemblies can occur via two principal mechanisms, olation (An-OH + (H_2O)-An ↔ An-OH-M + H_2O) and oxolation (An-OH + OH-An ↔ An-O-M + H_2O), with the former being the relevant pathway for the present Pu(VI) case [36].

Such apparent links between trimeric solution species as building blocks and solid-phase structures can also be stated for some classical U(VI) oxide compounds. The trimer described by Åberg, $[(UO_2)_3O(OH)_3(H_2O)_6](NO_3)(H_2O)$, represents the most explicit example, with the aqueous (3,5) hydrolysis complex $(UO_2)_3(\mu_3\text{-O})(\mu_2\text{-OH})_3(t\text{-}H_2O)_6^{+}$ crystallized as a finite cluster [37]. For other U(VI) compounds the link is less obvious but can still be argued. Examples are the class of U(VI)-O(H) minerals with sheet anion topologies consisting of triangles and pentagons, for example metaschoepite $[(UO_2)_4O(OH)_6](H_2O)_5$, becquerelite $Ca[(UO_2)_3O_2(OH)_3]_2(H_2O)_8$) and fourmarierite $Pb_{1.57}[(UO_2)_{10}O_6(OH)_{11}](H_2O)_{11}$ [14]. Their synthetic analogues typically form in aqueous solutions under slightly acidic pH at high initial U(VI) concentrations, that is, under conditions where the trimeric (3,5) complex $(UO_2)_3(OH)_5^{+}$ is highly relevant together with mononuclear UO_2^{2+}, $UO_2(OH)^{+}$ and dinuclear $(UO_2)_2(OH)_2^{2+}$ [25, 38–41]. Thus, the formation of these phases can be interpreted to be largely the result of a condensation of the trimeric uranyl precursors in solution, and remnants of the precursor may be identified in the resulting topologies.

As larger Pu(VI) and Np(VI) oxide clusters are not reported, the closest comparison to **(I)** and **(II)** is the U(VI) peroxide cage cluster system [9–11]. Several substantial differences between the U(VI)-O_2 and the present {Pu_{60}} cage clusters are noteworthy. Firstly, the latter are based solely on oxido and hydroxo as bridging ligands and contain exclusively pentagonal bipyramidal Pu(VI) moieties. Burns et al. also pointed out that the relevance of the side-on bonded peroxide in U(VI)-O_2 cages is not only related to the pliability of the U(VI)-O_2-U(VI) bridges but also to the limitation of the number of connections to neighboring uranyl polyhedra [11]. Both properties are fulfilled by the trimeric subunits in the {Pu_{60}} clusters, classifying their aqueous precursor molecules—here the divalent (3,8) solution complex—as a new class of fundamental building blocks in actinide cage cluster chemistry. The fact that **(I)** and **(II)** form in simple aqueous NaCl-NaOH solutions highlights their principal relevance for Pu-containing systems in alkaline, oxidizing milieu.

Our results also provide insight into why the formation of larger U(VI) cage clusters with An ≥ 16 based solely on (hydr)oxide ligands is challenging. The formation of **(I)** and **(II)** occurs in highly alkaline conditions where the anionic trimeric

25109537, 2026, 1, Downloaded from https://onlinelibrary.wiley.com/doi/10.1002/anov.70018, Wiley Online Library on [09/04/2026]. See the Terms and Conditions (https://onlinelibrary.wiley.com/terms-and-conditions) on Wiley Online Library for rules of use; OA articles are governed by the applicable Creative Commons License

Pu(VI)-O(H) solution species (precursor) are long-term metastable and present at high concentrations. U(VI) as well as Np(VI) undergo immediate precipitation starting at near-neutral pH, typically leading to the formation of layered oxy-hydroxide phases. These phases limit U(VI)/Np(VI) concentrations by solubility equilibria to lower values than are achievable in the metastable Pu(VI)-OH system, reducing the probability of forming U(VI)/Np(VI) aqueous trimers—especially an analog divalent (3,8) species. Indeed, the mononuclear $AnO_2(OH)_3^-$ and $AnO_2(OH)_4^{2-}$ are predominant in most solubility-controlled U(VI)/Np(VI) systems [25].

Finally, it is interesting to note that the formation of dark-brown crystals with rod- and plate-like shapes precipitating from metastable Pu(VI)(aq) systems in the presence of 0.5 M NaOH and with an initial Pu(VI) inventory of about 200 µg—that is, closely resembling the building conditions of **(I)** and **(II)** in the present work—was already reported in one of the earliest studies on Pu(VI)(aq) chemistry performed during the Manhattan Project [42]. However, with the exception of optical-microscopic inspection and an oxidation state analysis, no additional characterization was described. Possible reasons might be the peculiar mechanical instability of the material, allowing compounds **(I)** and **(II)** to easily disappear or redissolve during handling operations such as washing steps, as well as the challenges related to crystallographic analysis of large-unit-cell clusters that were difficult to manage with the methods at that time. Our results provide a compelling contribution to closing the unresolved issue.

3 | Conclusion

The present work opens interesting options for future research into the fascinating topic of inorganic actinide cage cluster chemistry, for example, analyzing the impact of different synthesis conditions on the Pu(VI) cage cluster structure, exploring the potential existence of analogous U(VI) and Np(VI) compounds and trends within the An(VI) series, and applying dedicated spectroscopic and thermodynamic techniques. As both An(VI) and An(V) intrinsically grant access to pentagonal structural motifs, investigations into the redox properties of the Pu(VI) clusters aiming at the formation of similar Pu(V) compounds are also interesting perspectives. Finally, our work highlights that an in-depth understanding of metal solution speciation and thermodynamics strongly facilitates investigations into self-assembled systems.

Acknowledgments

The authors thank the Institute for Beam Physics and Technology (IBPT, KIT) for the operation of the storage ring, the Karlsruhe Research Accelerator (KARA), and Volker Krepper (KIT-INE) for technical support.

Conflicts of Interest

The authors declare no conflicts of interest.

Data Availability Statement

The data that supports the findings of this study are available in the supplementary material of this article.

References

1. S. Dehnen, ed., *Clusters—Contemporary Insight in Structure and Bonding* 174 (Springer, 2017).

2. A. V. Virovets, E. Peresypkina, and M. Scheer, "Structural Chemistry of Giant Metal Based Supramolecules," *Chemical Reviews* 121 (2021): 14485–14554, https://doi.org/10.1021/acs.chemrev.1c00503.

3. M. T. Pope and A. Müller, "Polyoxometalate Chemistry: An Old Field With New Dimensions in Several Disciplines," *Angewandte Chemie International Edition in English* 30 (1991): 34–48, https://doi.org/10.1002/anie.199100341.

4. L. Cronin and A. Müller, "Themed Issue on Latest Developments in Polyoxometalate Science," *Chemical Society Reviews* 41 (2012): 7325–7648.

5. N. I. Gumerova and A. Rompel, "Polyoxometalates in Solution: Speciation Under Spotlight," *Chemical Society Reviews* 49 (2020): 7568–7601, https://doi.org/10.1039/D0CS00392A.

6. X.-M. Luo, Y.-K. Li, X.-Y. Dong, and S.-Q. Zang, "Platonic and Archimedean Solids in Discrete Metal-Containing Clusters," *Chemical Society Reviews* 52 (2023): 383–444, https://doi.org/10.1039/D2CS00582D.

7. G.-P. Yang, K. Li, and C.-W. Hu, "Recent Advances in Uranium-Containing Polyoxometalates," *Inorganic Chemistry Frontiers* 9 (2022): 5408–5433, https://doi.org/10.1039/D2QI01834A.

8. P. C. Burns, K.-A. Kubatko, G. Sigmon, et al., "Actinyl Peroxide Nanospheres," *Angewandte Chemie International Edition* 44 (2005): 2135–2139, https://doi.org/10.1002/anie.200462445.

9. J. Qiu and P. C. Burns, "Clusters of Actinides With Oxide, Peroxide, or Hydroxide Bridges," *Chemical Reviews* 113 (2013): 1097–1120, https://doi.org/10.1021/cr300159x.

10. P. C. Burns and M. Nyman, "Captivation With Encapsulation: A Dozen Years of Exploring Uranyl Peroxide Capsules," *Dalton Transactions* 47 (2018): 5916–5927, https://doi.org/10.1039/C7DT04245K.

11. S. Hickam and P. C. Burns, "Oxo Clusters of 5f Elements," *Structure and Bonding* 173 (2017): 121–154.

12. G. R. Choppin, "Utility of Oxidation State Analogs in the Study of Plutonium Behavior," *Radiochimica Acta* 85 (1999): 89–95.

13. T. Fanghänel and V. Neck, "Aquatic Chemistry and Solubility Phenomena of Actinide Oxides/Hydroxides," *Pure and Applied Chemistry* 74 (2002): 1895, https://doi.org/10.1351/pac200274101895.

14. A. J. Lussier, R. A. K. Lopez, and P. C. Burns, "A Revised and Expanded Structure Hierarchy of Natural and Synthetic Hexavalent Uranium Compounds," *The Canadian Mineralogist* 54 (2016): 177, https://doi.org/10.3749/canmin.1500078.

15. D. L. Clark, D. A. Geeson, and R. J. Hanrahan, *Plutonium Handbook*, 2nd edition (American Nuclear Society, 2019).

16. D. L. Clark, "The Chemical Complexities of Plutonium," *Los Alamos Science* 26 (2000): 364–381.

17. L. Soderholm, P. M. Almond, S. Skanthakumar, R. E. Wilson, and P. C. Burns, "The Structure of the Plutonium Oxide Nanocluster [Pu38O56Cl54(H2O)8]14−," *Angewandte Chemie International Edition* 47 (2008): 298–302.

18. R. E. Wilson, S. Skanthakumar, and L. Soderholm, "Separation of Plutonium Oxide Nanoparticles and Colloids," *Angewandte Chemie International Edition* 50 (2011): 11234–11237, https://doi.org/10.1002/anie.201105624.

19. C. Falaise, C. Volkringer, J.-F. Vigier, et al., "Isolation of the Large {Actinide}38 Poly-oxo Cluster With Uranium," *Journal of the American Chemical Society* 135 (2013): 15678, https://doi.org/10.1021/ja4067207.

20. N. P. Martin, C. Volkringer, P. Roussel, et al., "{Np38} Clusters: The Missing Link in the Largest Poly-oxo Cluster Series of Tetravalent Actinides," *Chemical Communications* 54 (2018): 10060, https://doi.org/10.1039/C8CC03744B.

25109537, 2026, 1, Downloaded from https://onlinelibrary.wiley.com/doi/10.1002/anov.70018, Wiley Online Library on [09/04/2026]. See the Terms and Conditions (https://onlinelibrary.wiley.com/terms-and-conditions) on Wiley Online Library for rules of use; OA articles are governed by the applicable Creative Commons License

21. K. A. Kraus and J. R. Dam, "Hydrolytic Behavior of Plutonium(VI) Acid-Base Titrations of Plutonium(VI)" Paper 4.18 in the Transuranium Elements," (McGraw-Hill, 1949).

22. A. Cassol, L. Magon, L. R. Portanova, and E. Tondello, "Hydrolysis of Plutonium(VI): Acidity Measurements in Perchlorate Solutions," *Radiochimica Acta* 17 (1972): 28–32.

23. I. Pashalidis, (Technical University of Munich (DE), 1992).

24. L. Rao, G. Tian, P. Di Bernardo, and P. Zanonato, "Hydrolysis of Plutonium(VI) at Variable Temperatures (283–343 K)," *Chemistry—A European Journal* 17 (2011): 10985–10993, https://doi.org/10.1002/chem.201100120.

25. I. Grenthe, X. Gaona, and A. V. Plyasunov, *Second Update on the Chemical Thermodynamics of Uranium, Neptunium, Plutonium, Americium and Technetium* (OECD Publications, 2020).

26. D. Fellhauer, O. Walter, R. Meier, et al., "Pu(VI) Hydrolysis in Aqueous NaCl-NaOH solutions," "Paper S1-A1, 19th International Conference on Chemistry and Migration Behavior of Actinides and Fission Products in the Geosphere—Migration 2025, Sep 21-26, 2025, New Orleans, LA, USA (related manuscript in preparation)".

27. These trimers are typically assigned as $(AnO_2)_3(OH)_5^+$ = (3,5) to $(AnO_2)_3(OH)_8^{2-}$ = (3,8), reflecting their total hydroxide contents as derived from macroscopic pH dependent studies like potentiometry—here, one oxido ligand has the same pH dependence as two hydroxides—rather than their exact structural properties, which is better expressed as $(AnO_2)_3(\mu_3\text{-}O)(\mu_2\text{-}OH)_3(t\text{-}OH)_x(t\text{-}H_2O)_{6-x}^{1-x}$ with x = 0-3.

28. Deposition numbers 2497915 (for I), and 2497916 (for II) contain the supplementary crystallographic data for this paper. These data are provided free of charge by the joint Cambridge Crystallographic Data Centre and Fachinformationszentrum Karlsruhe Access Structures service.

29. K. Momma and F. Izumi, "VESTA 3 for Three-Dimensional Visualization of Crystal, Volumetric and Morphology Data," *Journal of Applied Crystallography* 44 (2011): 1272–1276.

30. G. E. Sigmon, D. K. Unruh, J. Ling, et al., "Symmetry versus Minimal Pentagonal Adjacencies in Uranium-Based Polyoxometalate Fullerene Topologies," *Angewandte Chemie International Edition* 48 (2009): 2737–2740, https://doi.org/10.1002/anie.200805870.

31. J. Ling, C. M. Wallace, J. E. S. Szymanowski, and P. C. Burns, "Hybrid Uranium–Oxalate Fullerene Topology Cage Clusters," *Angewandte Chemie International Edition* 49 (2010): 7271–727340, https://doi.org/10.1002/anie.201003197.

32. W. Niu, W. Zhang, S. Firdoz, and X. Lu, "Dodecahedral Gold Nanocrystal: The Missing Platonic Shape," *Journal of the American Chemical Society* 17 (2014): 10985–10993.

33. J. A. McCleverty and T. J. Meyer, *Comprehensive Coordination Chemistry II* (Elsevier, 2003).

34. M. Nyman and T. M. Alam, "Dynamics of Uranyl Peroxide Nanocapsules," *Journal of the American Chemical Society* 134 (2012): 20131–20138, https://doi.org/10.1021/ja308673f.

35. D. Fellhauer, X. Gaona, J. Rothe, M. Altmaier, and T. Fanghänel, "Neptunium(VI) Solubility in Alkaline $CaCl_2$ Solutions: Evidence for the Formation of Calcium Neptunates Ca_xNpO_{3+x}(s,hyd)," *Monatshefte für Chemie- Chemical Monthly* 149 (2018): 237–252.

36. K. E. Knope and L. Soderholm, "Solution and Solid-State Structural Chemistry of Actinide Hydrates and Their Hydrolysis and Condensation Products," *Chemical Reviews* 113 (2013): 944–994, https://doi.org/10.1021/cr300212f.

37. M. Aberg, "The Crystal Structure of Hexaaqua-tri-mu-hydroxo-mu3-oxo-triuranyl(VI) Nitrate Tetrahydrate, $[(UO_2)_3O(OH)_3(H_2O)_6NO_3\cdot 4H_2O$," *Acta Chemica Scandinavica* 32a (1978): 101–107, https://doi.org/10.3891/acta.chem.scand.32a-0101.

38. M. Altmaier, E. Yalcintas, X. Gaona, et al., "Solubility of U(VI) in Chloride Solutions. I. The Stable Oxides/Hydroxides in NaCl Systems, Solubility Products, Hydrolysis Constants and SIT Coefficients," *The Journal of Chemical Thermodynamics* 114 (2017): 2–13, https://doi.org/10.1016/j.jct.2017.05.039.

39. M. C. A. Sandino and B. Grambow, "Solubility Equilibria in the U(VI)-Ca-K-Cl-H_2O System: Transformation of Schoepite Into Becquerelite and Compreignacite," *Radiochimica Acta* 66/67 (1994): 37–43.

40. D. Rai, A. R. Felmy, N. J. Hess, V. L. LeGore, and D. E. McCready, "Thermodynamics of the U(VI)-Ca^{2+}-Cl^--OH^--H_2O system: Solubility Product of becquerelite," *Radiochimica Acta* 90 (2002): 495–503.

41. Y. Li and P. C. Burns, "Investigations of Crystal-Chemical Variability in Lead Uranyl Oxide Hydrates. Ii. Fourmarierite," *The Canadian Mineralogist* 38 (2000): 737–749, https://doi.org/10.2113/gscanmin.38.3.737.

42. R. E. Connick, W. H. McVey, and G. E. Sheline, "Note on the Stability of Plutonium(VI) in Alkaline solution," in *The Transuranium Elements* (McGraw-Hill, 1949).

43. M. Altmaier, V. Metz, V. Neck, R. Müller, and T. Fanghänel, "Solid-liquid Equilibria of $Mg(OH)_2$(cr) and $Mg_2(OH)_3Cl\cdot 4H_2O$(cr) in the System Mg-Na-H-OH-Cl-H_2O at 25°C," *Geochimica Et Cosmochimica Acta* 67, no. 19 (2003): 3595–3601, https://doi.org/10.1016/S0016-7037(03)00165-0.

44. K. S. Pitzer, *Activity Coefficients in Electrolyte Solutions* (CRC Press, 1991).

45. H. Nitsche, S. C. Lee, and R. C. Gatti, "Determination of Plutonium Oxidation States at Trace Levels Pertinent to Nuclear Waste Disposal," *Journal of Radioanalytical and Nuclear Chemistry* 124 (1988): 171–185, https://doi.org/10.1007/BF02035515.

46. *SAINT, SADABS*; Siemens 1997, Analytical X-ray Instruments Inc., Karlsruhe, Germany.

47. G. M. Sheldrick, "A Short History of SHELX," *Acta Crystallographica* 64 (2008): 112–122, https://doi.org/10.1107/S0108767307043930.

48. J. Rothe, M. Altmaier, R. Dagan, et al., "Fifteen Years of Radionuclide Research at the KIT Synchrotron Source in the Context of the Nuclear Waste Disposal Safety Case," *Geosciences* 9 (2019): 91, https://doi.org/10.3390/geosciences9020091.

49. B. Ravel and M. Newville, "ATHENA, ARTEMIS, HEPHAESTUS: Data Analysis for X-ray Absorption Spectroscopy IFEFFIT," *Journal of Synchrotron Radiation* 12 (2005): 537–541, https://doi.org/10.1107/S0909049505012719.

50. A. L. Ankudinov, C. Bouldin, J. J. Rehr, J. Sims, and H. Hung, "Parallel Calculation of Electron Multiple Scattering Using Lanczos Algorithms," *Physical Review B* 65 (2002): 104107, https://doi.org/10.1103/PhysRevB.65.104107.

51. D. Cohen, "The Absorption Spectra of Plutonium Ions in Perchloric Acid Solutions," *Journal of Inorganic and Nuclear Chemistry* 18 (1961): 211–218, https://doi.org/10.1016/0022-1902(61)80390-4.

52. T. Vitova, I. Pidchenko, D. Fellhauer, et al., "The Role of the 5f Valence Orbitals of Early Actinides in Chemical Bonding," *Nature Communications* 8 (2017): 16053, https://doi.org/10.1038/ncomms16053.

53. C. Walther, J. Rothe, B. Brendebach, et al., "New Insights in the Formation Processes of Pu(IV) Colloids," *Radiochimica Acta* 97 (2009): 199–207, https://doi.org/10.1524/ract.2009.1595.

54. A. Fischer, "Competitive Coordination of the Uranyl Ion by Perchlorate and Water - the Crystal Structures of $UO_2(ClO_4)_2\cdot 3H_2O$ and $UO_2(ClO_4)_2\cdot 5H_2O$ and a Redetermination of $UO_2(ClO_4)_2\cdot 7H_2O$," *Journal of Inorganic and General Chemistry* 629 (2003): 1012–1016, https://doi.org/10.1002/zaac.200200450.

55. M. Åberg, L. Nilson, C. Larsen, et al., "The Crystal Structure of $[(UO_2)_2(OH)_2Cl_2(H_2O)_4]$," *Acta Chemica Scandinavica* 23 (1969): 791–810, https://doi.org/10.3891/acta.chem.scand.23-0791.

56. M. T. Weller, M. E. Light, and T. Gelbrich, "Structure of Uranium(VI) Oxide Dihydrate, $UO_3\cdot 2H_2O$; Synthetic Meta -schoepite

25109537, 2026, 1, Downloaded from https://onlinelibrary.wiley.com/doi/10.1002/anov.70018, Wiley Online Library on [09/04/2026]. See the Terms and Conditions (https://onlinelibrary.wiley.com/terms-and-conditions) on Wiley Online Library for rules of use; OA articles are governed by the applicable Creative Commons License

$(UO_2)_4O(OH)_6{\cdot}5H_2O$," *Acta Crystallographica Section B: Structural Science, Crystal Engineering, and Materials* 56 (2000): 577–583, https://doi.org/10.1107/S0108768199016559.

57. P. C. Burns and Y. P. Li, "The Structures of Becquerelite and Sr-exchanged Becquerelite," *American Mineralogist* 87 (2002): 550–557, https://doi.org/10.2138/am-2002-0418.

58. P. C. Burns, "A New Uranyl Oxide Hydrate Sheet in Vandendriesscheite; Implications for Mineral Paragenesis and the Corrosion of Spent Nuclear Fuel," *American Mineralogist* 82 (1997): 1176–1186, https://doi.org/10.2138/am-1997-11-1214.

59. C. Dion, S. Obbade, E. Raekelboom, F. Abraham, and M. Saadi, "Synthesis, Crystal Structure, and Comparison of Two New Uranyl Vanadate Layered Compounds: $M_6(UO_2)_5(VO_4)_2O_5$ With M=Na, K," *Journal of Solid State Chemistry* 155 (2000): 342–353, https://doi.org/10.1006/jssc.2000.8923.

60. S. Obbade, C. Dion, L. Duvieubourg, M. Saadi, and F. Abraham, "Synthesis and Crystal Structure of α and β-$Rb_6U_5V_2O_{23}$, a New Layered Compound," *Journal of Solid State Chemistry* 173 (2003): 1–12, https://doi.org/10.1016/S0022-4596(03)00052-5.

61. J. D. Woodward and T. E. Albrecht-Schmitt, "Molten Salt Flux Synthesis and Structure of the New Layered Uranyl Tellurite, $K_4[(UO_2)_5(TeO_3)_2O_5]$," *Journal of Solid State Chemistry* 178 (2005): 2922–2926, https://doi.org/10.1016/j.jssc.2005.06.043.

62. D. L. Clark, S. D. Conradson, R. J. Donohoe, et al., "Chemical Speciation of the Uranyl Ion Under Highly Alkaline Conditions. Synthesis, Structures, and Oxo Ligand Exchange Dynamics," *Inorganic Chemistry* 38 (1999): 1456–1466, https://doi.org/10.1021/ic981137h.

63. U. Wahlgren, H. Moll, I. Grenthe, et al., "Structure of Uranium(VI) in Strong Alkaline Solutions. A Combined Theoretical and Experimental Investigation," *Journal of Physical Chemistry A* 103 (1999): 8257–8264, https://doi.org/10.1021/jp990042d.

64. D. L. Clark, S. D. Conradson, R. J. Donohoe, et al., "Chemical Speciation of Neptunium(VI) Under Strongly Alkaline Conditions. Structure, Composition, and Oxo Ligand Exchange," *Inorganic Chemistry* 52 (2013): 3547–3555, https://doi.org/10.1021/ic3020139.

Supporting Information

Additional supporting information can be found online in the Supporting Information section.

Caution! Plutonium is a strongly radioactive and highly toxic heavy metal. Appropriate pre-cautions were taken when handling Pu solutions. Experiments with plutonium were carried out under inert argon atmosphere using glovebox techniques inside the radioactive controlled areas of the Karlsruhe Institute of Technology—Institute for Nuclear Waste Disposal and the Joint Research Centre Karlsruhe. Compounds (I) and (II) were characterized by SC-XRD, XAFS, SEM-EDX, Vis/NIR studies. Details are summarized in the Supplementary Information. The authors have cited additional references within the Supporting Information [43–64].

25109537, 2026, 1, Downloaded from https://onlinelibrary.wiley.com/doi/10.1002/anov.70018, Wiley Online Library on [09/04/2026]. See the Terms and Conditions (https://onlinelibrary.wiley.com/terms-and-conditions) on Wiley Online Library for rules of use; OA articles are governed by the applicable Creative Commons License